Unsupervised Wave Physics-Informed Representation Learning for Guided Wavefield Reconstruction

Joel B. Harley¹, Benjamin Haeffele², and Harsha Vardhan Tetali¹

 1 University of Florida, Gainesville FL 32603, USA 2 Mathematical Institute for Data Science, Johns Hopkins University, Baltimore MD, 21218 $\tt lncs@springer.com$

Abstract. Ultrasonic guided waves enable us to monitor large regions of a structure at one time. Characterizing damage through reflection-based and tomography-based analysis or by extracting information from wavefields measured across the structure is a complex dynamic-data driven applications system (DDDAS). As part of the measurement system, guided waves are often measured with in situ piezoelectric sensors or wavefield imaging systems, such as a scanning laser doppler vibrometer. Adding sensors onto a structure is costly in terms of components, wiring, and processing and adds to the complexity of the DDDAS while sampling points with a laser doppler vibrometer requires substantial time since each spatial location is often averaged to minimize perturbations introduced by dynamic data. To reduce this burden, several approaches have been proposed to reconstruct full wavefields from a small amount of data. Many of these techniques are based on compressive sensing theory, which assumes the data is sparse in some domain. Among the existing methods, sparse wavenumber analysis achieves excellent reconstruction accuracy with a small amount of data (often 50 to 100 measurements) but assumes a simple geometry (e.g., a large plate) and assumes knowledge of the transmitter location. This is insufficient in many practical scenarios since most structures have many sources of reflection. Many other compressive sensing methods reconstruct wavefields from Fourier bases. These methods are geometry agnostic but require much more data (often more than 1000 measurements). This paper demonstrates a new DDDAS approach based on unsupervised wave physics-informed representation learning. Our method enables learning full wavefield representations of guided wave datasets. Unlike most compressive sensing methodologies that utilize sparsity in some domain, the approach we developed in our lab is based on injecting wave physics into a low rank minimization algorithm. Unlike many other learning algorithms, including deep learning methods, our approach has global convergence guarantees and the low rank minimizer enables us to predict wavefield behavior in unmeasured regions of the structure. The algorithm can also enforce the wave equation across space, time, or both dimensions simultaneously. Injecting physics also provides the algorithm tolerance to data perturbations. We demonstrate the performance of our algorithm with experimental wavefield data from a 1m by 1m region of an aluminum plate with a half-thickness notch in its center.

Keywords: DDDAS, wave-informed machine learning, signal processing, acoustics

1 Introduction

1.1 Overview

Structural health monitoring is a Dynamic Data Driven Applications System (DDDAS) in which the characteristics of a structure or material dynamically vary over time due to gradual growth of damage as well as other environmental and operational variations. All these changes affect our sensor systems. Ultrasonic guided waves are a common sensing modality in structural health monitoring that allow us to characterize and identify damage in large regions of structures [1], [2]. Guided waves can be measured with in situ piezoelectric sensors or wavefield imaging systems, such as scanning laser Doppler vibrometers [3]. Even with a full wavefield imaging system, characterizing and understanding guided wave propagation can be challenging. This is due to their frequency-dependent propagation and complex interactions with structural components [4]. As a result, significant efforts have been dedicated to advanced algorithms and techniques for analyzing and characterizing guided wave data. Specifically, this paper aims to obtain compact representations of guided wave data that characterize the propagation environment with minimal assumptions. We only assume the wave equation is satisfied and based on the theory presented in [5]. Minimal assumptions are necessary in many scenarios since we often have minimal knowledge about the environment and no knowledge about the damage and its effects on the guided waves propagation.

Guided wave data has been analyzed through reflection-based [6]-[8], tomographybased [9], and wavefield-based analysis methods [3], [10]. Several wavefield analysis methods learn or extract special representations of the wavefields. These representations may have a physical basis, such as the modal dispersion curves [11] of guided waves, which characterize based on the material properties (e.g., velocities, densities, and thickness) and on known physics. Among these methods, sparse wavenumber analysis can extract dispersion curves with limited data [12], [13]. Most of these methods utilize a large pool of representations (often represented by a matrix) based on an analytical solution to the problem at hand (as in [14]). Yet, these fail for two reasons. First, the space of possible solutions is often infinite. In the case of the wave equation, for example, we may have one or more real-valued wavenumbers and/or frequencies that must be identified. Estimating these values is often not trivial. More importantly, there are many known representations that solve a differential equation [13], [15] but may not be compact for the specific problem, thereby becoming an ineffective representation. For example, the Fourier representation is always a solution to the wave equation [16], [17]. Yet, in the presence of discontinuities in time or space, it is not a compact representation as an infinite number of Fourier components are required. Hence, structural health monitoring systems cannot effectively represent cracks or delaminations with a Fourier basis.

There are past also efforts to integrate physics into other data-driven models. In addition, data assimilation methods used in time-series forecasting often inject physics into

their frameworks [18] and act in conjunction with powerful, but often constrained, models to predict the future state of a system. This is related to, but separate, from the approach in this paper, where we aim to learn the underlying characteristics / representations of the data or environment. These representations could be used to highlight variations in such a time series, enabling us to integrate our approach with data assimilation strategies. Full waveform inversion (FWI) [19]similarly computes the characteristics of the environment based on a chosen physical model. However, the physical models used in FWI are highly constrained (i.e., often requiring many built-in assumptions) and usually coupled with expensive finite difference methods.

In contrast with each of these methods that rely on highly constrained models, our only constraint is that the data must satisfy the wave equation. While there is similar prior work on enforcing wave-physics into a dictionary learning framework with sparsity constraints in [20], this approach lacks the *global optimality guarantees, convergence guarantees,* and *algorithmic interpretability* that are present in this paper [5], [21]. Hence, we present a method to characterize material properties as well as decompose data that has strong algorithmic guarantees and assumes only fundamental physical knowledge. In addition, our physics-based decomposition can isolate and show how different wave modes propagate and change in the wavefield. We refer to our approach as wave-informed regression. We demonstrate this DDDAS approach with simulated wavefield data from a 1m by 1m region of an aluminum plate. The guided waves are generated by a 50 kHz frequency pulse.

2 WAVE-INFORMED REGRESSION METHODOLOGY

Wave-informed regression is based on learning a linear collection of modes that best represent wavefield data. These modes are learned by solving an optimization problem with three components: a mean squared error loss, a wave-informed loss, and mode number loss. We describe each of these components in the following subsections.

2.1 Mean Squared Error Loss

We represent a linear collection of modes to be learned as the columns of a matrix **D**. The sum of these modes reconstructs the wavefield. Hence, our first loss term minimizes the mean squared error between our reconstruction and wavefield data such that

$$c_{MSE} = \|\mathbf{x} - \mathbf{D1}\|_F^2$$

where the expression $\|\cdot\|_F^2$ represents the squared Frobenius norm, defined by the squared sum of all the matrix or vector elements. The full wavefield data \mathbf{x} is a vectorized form of a wavefield image \mathbf{X} at a single frequency ω

$$\mathbf{x} = \text{vec}(\mathbf{X}), \ \mathbf{X}_{i,i} = X(\omega, x_i, y_i).$$

For simplicity of notation, we assume the optimization is always performed at a single frequency ω . Each column of **D** represents a different vectorized spatial wave mode. The vector **1** represents a vector of all ones. Hence **D1** is the sum of columns in **D**. Note that without additional information, optimizing this loss is highly underdetermined – there exists an infinite number of possible solutions. Figure 1(a) illustrates an example of **X** around a center frequency of 50 kHz. We also illustrate this data in the wavenumber domain in Figure 1(b), with the axes representing the magnitudes of the horizontal and vertical wavenumbers. We can observe two modes of propagation at two distinct wavenumbers in these figures. However, it is difficult to observe that there is a spatial region with wavenumbers that are 10% higher than others. Hence, there are a total of four spatially dependent modes in this data.

2.2 Wave-Informed Loss

To obtain a meaningful modal representation, we add a loss function that represents the wave, or Helmholtz equation. The wave equation loss function is defined by

$$c_{\text{wave}} = \left\| \mathbf{L}_{x,y} \mathbf{D} - \mathbf{K} \mathbf{D} \right\|_{F}^{2}$$

where **K** is a diagonal matrix of squared wavenumbers k_m^2 . The matrix $\mathbf{L}_{x,y}$ represents an operator for the approximate second derivative in the x-direction added to the approximate second derivative in the y-direction. Note that each column of **D** is a vectorized image. The second derivative has multiple numerical approximations. In this paper, we use the second-order central difference approximation [22]. Note that this approximation is good for low frequencies (or wavenumbers) and poor for high frequencies (or wavenumbers). From a numerical perspective, a better second derivative operator can be obtained by stacking the discretized continuous eigen-functions corresponding to the continuous second derivative and computing a new Laplacian $\mathbf{L}_{x,y}$ using continuous eigen-values and eigen-functions.

2.3 Mode Number Loss

Adding the two previously discussed loss functions there are still many possible optimal **D** matrices, including Fourier-like matrices. Therefore, we consider the true solution to be the one that minimizes the number of modes by including a third cost:

$$c_{\text{size}} = \|\mathbf{D}\|_{\mathbf{F}}^2$$
.

Intuitively, when there are many modes, the Frobenius norm will be large. When there is a small number of modes, the Frobenius norm will be small. Therefore, minimizing this cost will simultaneously minimize the number of modes learned. We further refer to [23], which shows that penalizing the Frobenius norm is equivalent to penalizing the nuclear norm of the matrix (enforcing a sparsity in the number of bases). Hence, we choose $c_{\rm size}$ as the squared Frobenius norm, as in [5] since it helps in obtaining an

algorithm that solves the optimization problem to global optimality. Without this term, there would be many possible solutions to the optimization.

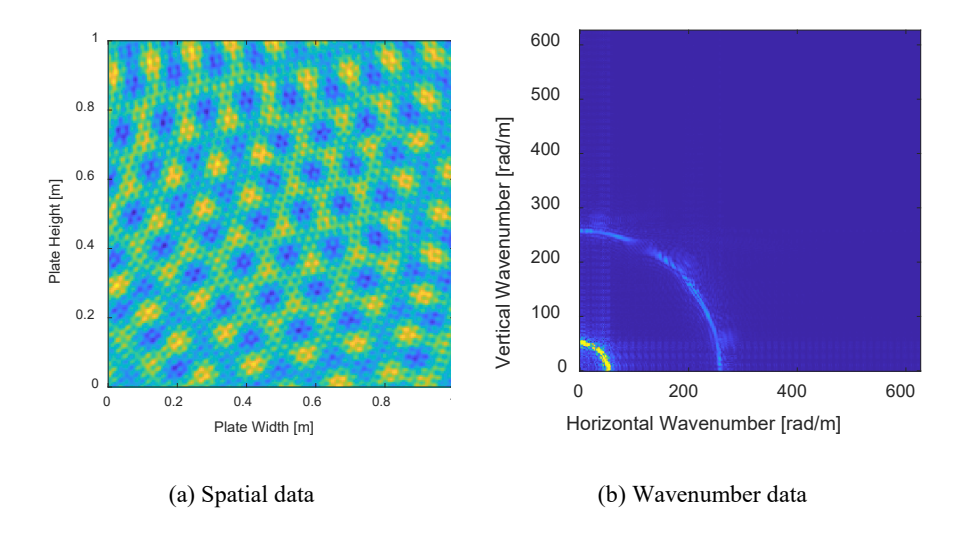


Fig. 1. Illustration of (a) single frequency spatial wavefield data and (b) the equivalent two-dimensional wavenumber domain. In (b), we observe two strong rings, representing the zeroth-order symmetric and zeroth-order asymmetric modes across the simulated plate.

2.4 Wave-informed Regression

When we add our costs together and incorporate regularization constants, we obtain

$$\min_{\textbf{D},\textbf{K},M}\lVert \textbf{x} - \textbf{D}\textbf{1} \rVert_F^2 + \lambda \bigg(\lVert \textbf{D} \rVert_F^2 + \frac{1}{\gamma^2}\lVert \textbf{L}\textbf{D} - \textbf{D}\textbf{K} \rVert_F^2 \bigg)$$

where M is the number of modes in the data. This formulation includes two regularization terms. The λ term represents a tradeoff between our mean squared error and our two regularizers while the γ^2 term represents the tradeoff between minimizing the number of modes and satisfying the wave equation.

2.5 Wave-Informed Algorithm

While we have established an optimization that defines wave-informed regression, creating an algorithm for solving this optimization is not trivial. This is because the optimization is not convex (i.e., there is more than one local minimum) and the variable to be optimized **D** is very high dimensional. As a result, there are no standard optimization algorithms that can be applied to this problem. An algorithm must be custom designed

to solve wave-informed regression. We briefly outline a simplified version of the algorithm that solves this optimization, detailed here [5], [20], [21]. In our version of the algorithm, we assume a fixed number of modes from the very start. The algorithm identifies each value of \mathbf{k}_i^2 in an iterative manner. After obtaining each \mathbf{k}_i^2 , it then updates **D**. Learning \mathbf{k}_i^2 is equivalent to learning an optimal filter in the wavenumber domain (see [5], [20], [21] for the exact connections to signal processing) and is closely related to standard estimation problems (specifically, spectral estimation [24]), only in our case we estimate both the modes and the wavenumbers. Learning **D** then combines and shapes these filters together to optimally reconstruct the data. Figure 2 outlines the algorithm in the form of a flowchart.

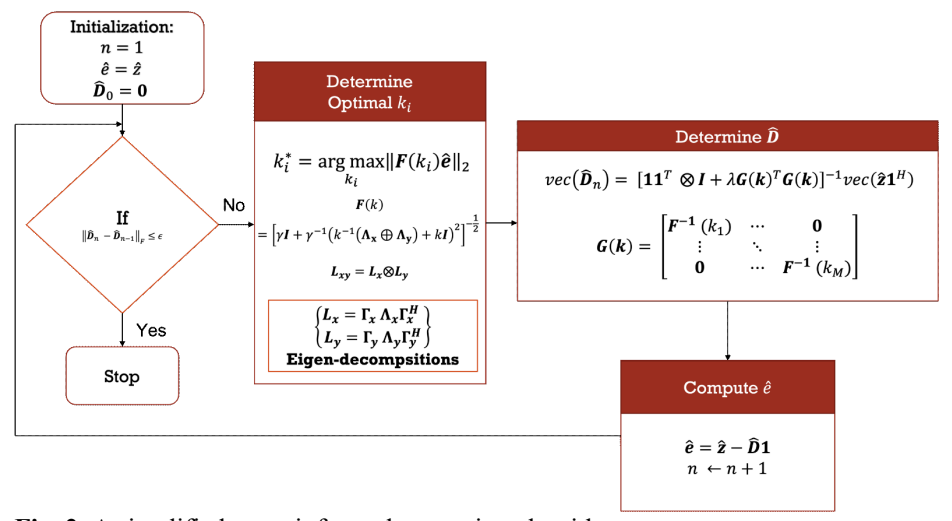
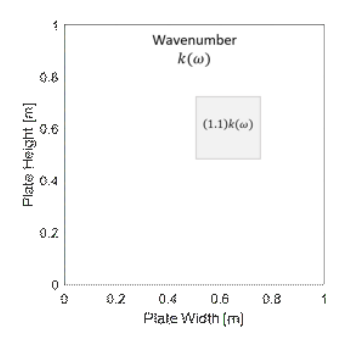


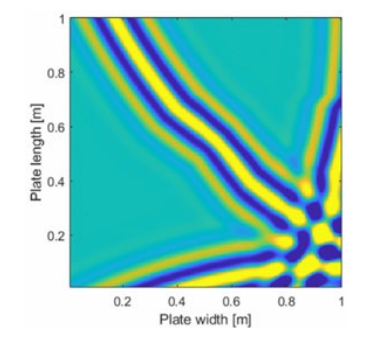
Fig. 2. A simplified wave informed regression algorithm

3 SIMULATION SETUP

We test our algorithm with a guided Lamb wave simulation. In the simulation, ultrasonic guided waves travel in multiple directions, originating from outside the frame. There is one region where the guided waves travel with a different wavenumber, which possibly represents delamination [25], corrosion [26], or complex structural elements [27]. The spatial frame is 1 m by 1 m with a grid spacing of 5 mm. We simulate two modes, the zeroth-order symmetric mode and the zeroth-order asymmetric mode. Two more modes are produced by our small region (shown in Figure 3(a)), which increases the wavenumbers by 10%. The guided wave data is simulated with a sampling rate of 1 MHz and a Gaussian transmission of 50 kHz center frequency and 25 kHz bandwidth. For wave-informed regression, we choose $\lambda = 1$ and $\gamma^2 = \pi^2/(N_x N_y)$, where $N_x N_y$ is the total number of elements in x. This defines γ as the width of one sample in the wavenumber domain. We choose to obtain M = 3 modes. Figure 3(b) illustrates an

snapshot of these waves at a single point in time. We know there are four modes in the data (A0 and S0 in the large and small regions). However, the S0 mode in the large region is difficult to distinguish from the S0 mode in the small region due to how similar the wavenumbers are.





- (a) Illustration of wavenumbers across the region of interest
- (b) Spatial wavefield data at one point in time

Fig. 3. Illustration of (a) the two different wavenumber regions present in our simulation setup and (b) a single-time snapshot of the S0 mode in our guided waves. The waves originate from three separate sources.

4 RESULTS

Figure 4 illustrates the first three modes extracted by wave-informed regression, in space and wavenumber. The second column illustrates that each mode corresponds to a particular wavenumber radius. The first column shows that the second mode is missing the small region with different wavenumbers. This region is observable in the third mode. The error for the wavenumbers estimated for each mode is 1.7 m⁻¹, 1 m⁻¹, and 2.3 m⁻¹, respectively. Overall, we demonstrate the ability to learn representations that spatially separate different modes or wavenumbers. We illustrate the results for two different points in time. The two points in time show the two different modes. The low wavenumber S0 mode is shown on the top and the high wavenumber A0 mode is shown on the bottom. As before, we see that the second mode has a spatial "hole" where the wavenumber changes, and the third mode fills that gap. Hence, we successfully extract the time-domain behavior of individual spatially varying modes.

5 CONCLUSIONS

This paper has illustrated preliminary results for wave-informed regression, a representation learning framework for combining wave physics within a DDDAS framework. The algorithm extracts the wavenumber of each mode in data as well as its spatially

varying components. The algorithm is unsupervised and therefore requires no prior training data. However, in the future, this approach can be applied to both supervised and unsupervised learning strategies. The benefits of these physics-informed learning techniques enable machine learning in structural health monitoring to be both more reliable as well as more interpretable and the algorithms are also not data hungry.

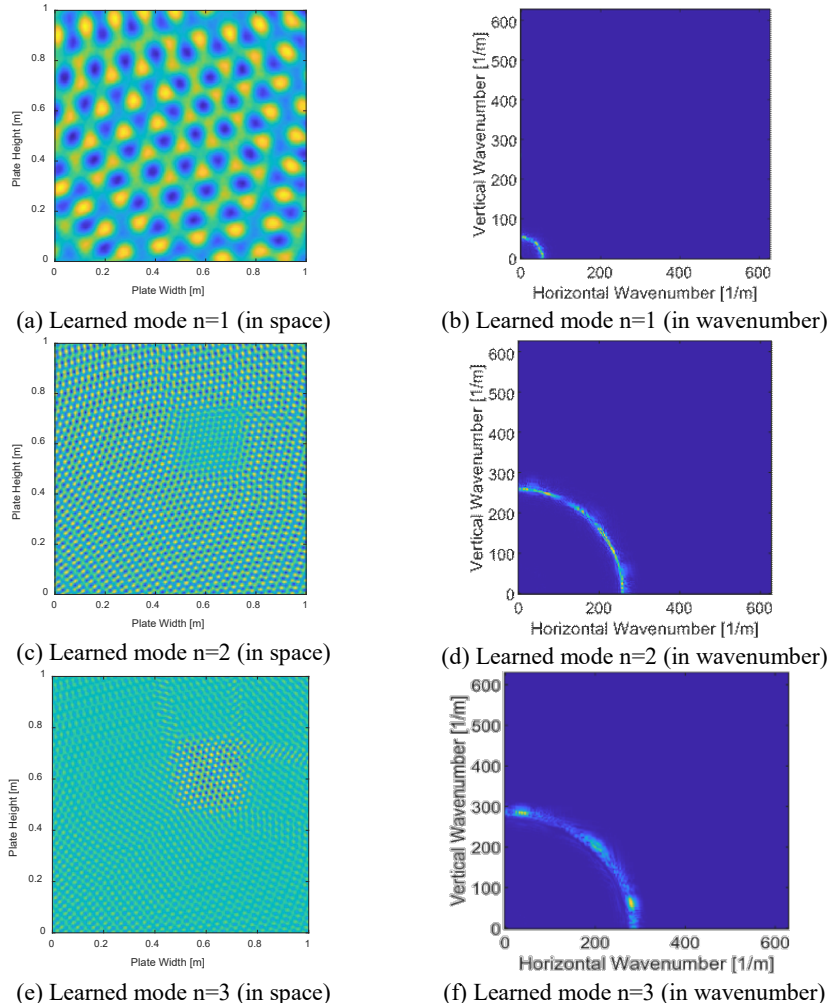


Fig. 4. Illustrations of the three modes (represented in the spatial and wavenumber domains) learned by wave-informed regression.

References

[1] P. Cawley, "Practical guided wave inspection and applications to structural health monitoring," in *Proc. of the Australasian Congress on Applied Mechanics*, Dec. 2007, p. 10.

- [2] J. Moll *et al.*, "Open Guided Waves: online platform for ultrasonic guided wave measurements," *Struct Health Monit*, vol. 18, no. 5–6, pp. 1903–1914, Nov. 2019, doi: 10.1177/1475921718817169.
- [3] W. J. Staszewski, B. C. Lee, L. Mallet, and F. Scarpa, "Structural Health Monitoring using Scanning Laser Vibrometry: I. Lamb Wave Sensing," *Smart Mater Struct*, vol. 13, no. 2, p. 251, Feb. 2004, doi: 10.1088/0964-1726/13/2/002.
- [4] A. J. Dawson, J. E. Michaels, and T. E. Michaels, "Isolation of ultrasonic scattering by wavefield baseline subtraction," *Mech Syst Signal Process*, vol. 70–71, pp. 891–903, Mar. 2016, doi: 10.1016/J.YMSSP.2015.09.008.
- [5] H. V. Tetali, J. B. Harley, and B. D. Haeffele, "Wave-Informed Matrix Factorization with Global Optimality Guarantees," *arXiv* [cs.LG], Jul. 2021, Accessed: Sep. 06, 2021. [Online]. Available: https://arxiv.org/abs/2107.09144v1
- [6] J. B. Harley and J. M. F. Moura, "Data-driven matched field processing for Lamb wave structural health monitoring," *Journal of the Acoustical Society of America*, vol. 135, no. 3, 2014, doi: 10.1121/1.4863651.
- [7] J. B. Harley, "Statistical lamb wave localization based on extreme value theory," in *Proc. of the Review of Progress in Quantitative Nondestructive Evaluation*, Jul. 2018, vol. 1949, p. 090004. doi: 10.1063/1.5031567.
- [8] A. Perelli, L. De Marchi, A. Marzani, and N. Speciale, "Frequency warped cross-wavelet multiresolution analysis of guided waves for impact localization," *Signal Processing*, vol. 96, no. PART A, pp. 51–62, Mar. 2014, doi: 10.1016/J.SIGPRO.2013.05.008.
- [9] J. Rao, M. Ratassepp, and Z. Fan, "Guided Wave Tomography Based on Full Waveform Inversion," *IEEE Trans Ultrason Ferroelectr Freq Control*, vol. 63, no. 5, 2016, doi: 10.1109/TUFFC.2016.2536144.
- [10] A. Sheremet, Y. Qin, J. P. Kennedy, Y. Zhou, and A. P. Maurer, "Wave Turbulence and Energy Cascade in the Hippocampus," *Front Syst Neurosci*, vol. 12, Jan. 2019, doi: 10.3389/fnsys.2018.00062.
- [11] J. B. Harley, A. C. Schmidt, and J. M. F. Moura, "Accurate sparse recovery of guided wave characteristics for structural health monitoring," in *Proc. of the IEEE International Ultrasonics Symposium*, Oct. 2012, pp. 158–161. doi: 10.1109/ULTSYM.2012.0039.
- [12] S. Sabeti and J. B. Harley, "Spatio-temporal undersampling: Recovering ultrasonic guided wavefields from incomplete data with compressive sensing," *Mech Syst Signal Process*, vol. 140, 2020, doi: 10.1016/j.ymssp.2020.106694.
- [13] K. S. S. Alguri, J. Melville, and J. B. Harley, "Baseline-free guided wave damage detection with surrogate data and dictionary learning," *J Acoust Soc Am*, vol. 143, no. 6, pp. 3807–3818, Jun. 2018, doi: 10.1121/1.5042240.
- [14] Z. Lai, I. Alzugaray, M. Chli, and E. Chatzi, "Full-field structural monitoring using event cameras and physics-informed sparse identification," *Mech Syst Signal Process*, vol. 145, p. 106905, Nov. 2020, doi: 10.1016/J.YMSSP.2020.106905.
- [15] O. Mesnil and M. Ruzzene, "Sparse wavefield reconstruction and source detection using Compressed Sensing," *Ultrasonics*, vol. 67, pp. 94–104, Apr. 2016, doi: 10.1016/J.ULTRAS.2015.12.014.

- [16] T. di Ianni, L. de Marchi, A. Perelli, and A. Marzani, "Compressive sensing of full wave field data for structural health monitoring applications," *IEEE Trans Ultrason Ferroelectr Freq Control*, vol. 62, no. 7, pp. 1373–1383, Jul. 2015, doi: 10.1109/TUFFC.2014.006925.
- [17] S. Sawant, S. Banerjee, and S. Tallur, "Performance evaluation of compressive sensing based lost data recovery using OMP for damage index estimation in ultrasonic SHM," *Ultrasonics*, vol. 115, p. 106439, Aug. 2021, doi: 10.1016/J.ULTRAS.2021.106439.
- [18] S. Ravela, "Two extensions of data assimilation by field alignment," *Lecture Notes in Computer Science (including subseries Lecture Notes in Artificial Intelligence and Lecture Notes in Bioinformatics)*, vol. 4487 LNCS, pp. 1147–1154, 2007, doi: 10.1007/978-3-540-72584-8_150.
- [19] R. Huang, Z. Zhang, Z. Wu, Z. Wei, J. Mei, and P. Wang, "Full-waveform inversion for full-wavefield imaging: Decades in the making," *The Leading Edge*, vol. 40, no. 5, pp. 324–334, May 2021, doi: 10.1190/TLE40050324.1.
- [20] H. V. Tetali, K. S. Alguri, and J. B. Harley, "Wave Physics Informed Dictionary Learning In One Dimension," in *Proc. of the IEEE International Workshop on Machine Learning for Signal Processing (MLSP)*, Oct. 2019, vol. 2019-Octob, pp. 1–6. doi: 10.1109/MLSP.2019.8918835.
- [21] H. V. Tetali, B. D. Haeffele, and J. B. Harley, "Wave physics-informed regression: Algorithm, interpretation, and application to wavefield imaging," *to be submitted*, 2023.
- [22] D. Yang, P. Tong, and X. Deng, "A central difference method with low numerical dispersion for solving the scalar wave equation," *Geophys Prospect*, vol. 60, no. 5, pp. 885–905, Jan. 2012, doi: 10.1111/J.1365-2478.2011.01033.X.
- [23] B. Recht, M. Fazel, and P. A. Parrilo, "Guaranteed minimum-rank solutions of linear matrix equations via nuclear norm minimization," *SIAM Review*, vol. 52, no. 3, pp. 471–501, Aug. 2010, doi: 10.1137/070697835.
- [24] S. L. Marple, "Tutorial overview of modern spectral estimation," *ICASSP*, *IEEE International Conference on Acoustics, Speech and Signal Processing Proceedings*, vol. 4, pp. 2152–2157, 1989, doi: 10.1109/ICASSP.1989.266889.
- [25] F. Gao, J. Hua, L. Wang, L. Zeng, and J. Lin, "Local wavenumber method for delamination characterization in composites with sparse representation of Lamb waves," *IEEE Trans Ultrason Ferroelectr Freq Control*, vol. 68, no. 4, pp. 1305–1313, Apr. 2021, doi: 10.1109/TUFFC.2020.3022880.
- [26] Z. Tian, W. Xiao, Z. Ma, and L. Yu, "Dispersion curve regression assisted wideband local wavenumber analysis for characterizing three-dimensional (3D) profile of hidden corrosion damage," *Mech Syst Signal Process*, vol. 150, p. 107347, Mar. 2021, doi: 10.1016/J.YMSSP.2020.107347.
- [27] J. Moll, T. Wandowski, P. Malinowski, M. Radzienski, S. Opoka, and W. Ostachowicz, "Experimental analysis and prediction of antisymmetric wave motion in a tapered anisotropic waveguide," *J Acoust Soc Am*, vol. 138, no. 1, p. 299, Jul. 2015, doi: 10.1121/1.4922823.